IRAQI JOURNAL OF APPLIED PHYSICS
Vol. 22, No. 3, July-September 2026, pp. 333-339

Studying Effect of Frequency on Capacitance–Resistance of Al/ITO/Al Humidity Sensor Prepared by Pulsed-Laser Deposition

Nisreen A. Fejer [1,2*]
Mohammed T. Hussein [3,4]
Asmaa H. Mohammed [2]

[1] College of Women Science, University of Baghdad, Baghdad, IRAQ
[2] College of Science, University of Al Nahrain, Baghdad, IRAQ
[3] College of Science, University of Baghdad, Baghdad, IRAQ
[4] AL Nukhba University College, Baghdad, IRAQ
* Corresponding author email: nisreen@csw.uobaghdad.edu.iq

Indium tin oxide (ITO) nanostructured films were deposited onto glass substrates using pulsed-laser deposition. The structure, shape, and optical properties of the deposited films were characterized. The ITO films were found to be polycrystalline with preferred at (222) crystal orientation (2θ=30.65°), and average crystallite size of about 23.22 nm when annealed at 200 °C for 60 minutes. The films exhibited an optical band gap around 3.4 eV due to the nanostructure formation and deposition method. The films showed uniform morphology with minimum surface roughness. They were also assessed for humidity sensing devices through capacitive-resistive method at the lower frequencies (100, 200, and 300 Hz) at room temperature. The results indicated that both resistance and capacitance were reduced with increasing frequency showing the possibility to employ the prepared films as efficient humidity sensor.

Keywords: Indium tin oxide; Thin films; Pulsed-laser deposition; Humidity sensor
Received: 28 August 2025; Revised: 28 October; Accepted: 4 November; Published: 1 July 2026

1. Introduction

Transparent conducting oxides (TCOs) are the materials that have attracted immense interest for a very unique blend of optical clearness and high electrical conductivity. These properties among others, make the TCOs indispensable materials for several applications, some of these include flat displays, solar cells, optoelectronics, and sensors [1-3]. While there are several TCO materials, the indium tin oxide (ITO) is the predominant choice, and this is due to the beneficial electrical and optical properties, stability at high temperatures, and the fact that it is usable with many deposition routes [4,5]. Nanotechnological advancements have also seen the scientists fabricate nanostructured ITO thin films with greatly extended functional abilities due to the enhanced surface to volume ratio and the fact that the microstructure is also tunable [6,7]. These attributes, typically in the literature, are particularly exciting for sensing applications, where surface phenomena are critical to device functioning or response time [8].

Humidity sensors are among the most developed sensor types as they have a vital impact on several areas such as industrial automation, environmental monitoring, medical diagnostics, and smart agriculture [9]. Humidity sensors work by recognizing changes in environmental water vapor and converting them to some measurable electrical signal (generally changes in frequency, capacitance, or resistance) [10].

Metal oxide (MO) semiconductors such as SnO_2, ZnO, and ITO are most recognized for their humidity sensing, as they have a high chemical stability, fast response time, and compatibility with thin film technologies [11,12]; more specifically, the adsorption and desorption of water molecules on the oxide surface affects the charge density carrier and subsequently regulates the balance of electrical conductivity of the sensor [13]. Pulsed-laser deposition (PLD) and drop casting techniques are the most well-studied deposition techniques for humidity sensors, as they provide exact control of important variables, such as crystallinity, surface morphology, and film thickness decoration, which influence humidity sensitivity and stabilization [14-16]. There are still challenges towards high sensitivity and long-term stability at room temperature and low power consumption, and that is why ITO-based humidity sensors will still be studied and researched as these problems are solved [17].

In this work, nanostructured ITO thin films were prepared using the PLD technique and extensively characterized using XRD, SEM, AFM, EDX, and UV-visible spectroscopy. The optical band gap was evaluated, and the films were tested as humidity sensors by measuring their capacitance-resistance

 © ALL RIGHTS RESERVED

response at different low frequencies under varying levels of relative humidity (RH%) at room temperature.

2. Materials and Methods

Indium tin oxide (ITO) nanopowder (99.99% pure, from Hongwu International Group) with an average particle size (APS) of 50 nm and a spherical shape was used to grow thin films of ITO on glass substrates via the pulsed-laser deposition (PLD) method. A Q-switched Nd:YAG laser (Huafei Tongda Technology-DIAMOND-28-pattern EPLS) with a fundamental wavelength of 1.06 μm and a pulse energy of 800 mJ with a 10 ns pulse duration and 6 Hz repetition rate was used for the deposition process. In addition, the laser system includes a power supply, a computer control, a cooling system, and a light route system. A light route system was set up in a handpiece, but the cooling, controlling, and power supply systems were installed in a machine box related to the power supply. The deposition process was carried out under vacuum pressure of 10^{-3} Torr and at room temperature to allow uniform and consistent growth of the thin film. After the films were deposited, they were post-annealed at 200 °C for 60 minutes to improve their structure and crystallinity.

The X-ray diffraction was used to examine the structural properties, and the results were then compared to the corresponding powder XRD patterns. The UV-visible spectrophotometer was also used to investigate the optical properties. The surface microstructure and morphology were further investigated through atomic force microsopy (AFM) and scanning electron microscopy (SEM), respectively. Energy-dispersive X-ray spectroscopy (EDX) was performed to determine the elemental analysis of the prepared samples.

The dimensions of the substrate utilized for the thin film deposition of $InSnO_2$ was 3x2 cm^2. The substrate, before the deposition process, was subjected to a cleaning process with the use of distilled water to rid the surface of any element or remnant matter. The substrate then went through an ultrasonic bath for 5 minutes with ethanol and then dried to ready it for the deposition process for the films.

The optical band gap value was measured, and the films were found to be characterized as humidity sensors through the resistance-capacitance response measurement under various relative humidity levels (RH) with the findings indicating the potential of PLD-deposited ITO films to be effective, room-temperature, rapid, and reversible humidity sensors.

Optical interferometry using fringe analysis was used to measure the thickness of ITO thin films accurately. This method is non-destructive and uses a coherent monochromatic light source, typically a He-Ne laser with wavelength 632.8 nm icident at an angle (usually 45°) with respect to the film surface [18]. Because the laser beam is partially reflected from the top surface of the ITO film and partially reflected from the interface between the film and substrate, an interference pattern is created by alternating bright and dark fringes. The spacing (fringe width) between the fringes contains critical information regarding the thickness of the ITO film. The thickness (t) of the ITO film can be calculated using the following equation [19,20]:

$$t = \frac{\lambda}{2}\frac{\Delta x}{X} \quad (1)$$

where λ is the laser wavelength, X is the fringes width, and Δx is the distance between interference fringes

Figure (1) shows a schematic diagram of the Al/ITO/Al film structure used as a humidity sensor. The capacitor plates and ohmic contact, represented by the aluminum substrate, were prepared using an aluminum wire of 99.99% purity. Aluminum electrodes of thickness 114 nm were deposited on a thoroughly cleaned glass substrate by the vacuum thermal evaporation method using a Balzer type BAE 370 unit with a boat-substrate distance 16.8cm under vacuum of approximately 10^{-5} mbar. The deposition rate of aluminum films were about 22 nm/min. To create gaps in the electrodes for the capacitive-humidity sensor substrate, a sharp blade was used to scratch the thin aluminum films. To measure the width of the formed gaps, an optical microscope was used, and it was found to be approximately 40 μm wide and then filled with ITO by PLD method (100 shots of laser pulse which is equally to 33nm). The effect of humidity on the electrical properties of the fabricated material was investigated by measuring the capacitance-resistance of the samples at room temperature with three different frequencies of the applied voltage (100, 200, and 300 Hz).

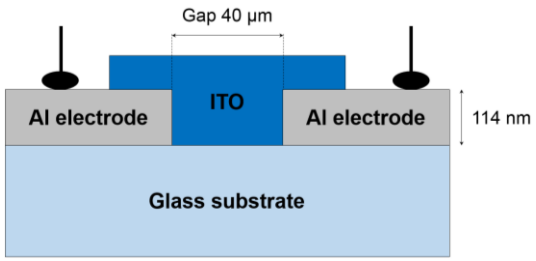

Fig. (1) Schematic diagram of Al/ITO/Al humidity sensor device

3. Results and Discussion

In this investigation, several tests were performed to determine the results of the optical properties, XRD, and surface morphology of various samples prepared by pulsed-laser deposition (PLD).

Elemental analysis was performed using EDX at an accelerating voltage of 20 kV and a magnification of 100x, as shown in Fig. (2). The sample was imaged using secondary electrons (SE), with a scale bar of 200 μm, allowing for the spatial resolution of the elemental distribution.

 © ALL RIGHTS RESERVED

Figure (3) shows that there was a lot of indium, as expected from ITO. Distinct peaks matching indium as well as other peaks matching tin and oxygen were seen. Some small peaks probably caused by the sample substrate were also found.

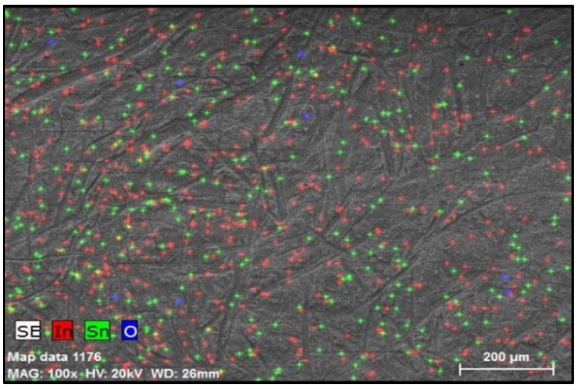

Fig. (2) EDX elemental map showing distribution of In (red), Sn (green), and O (blue), on the sample surface

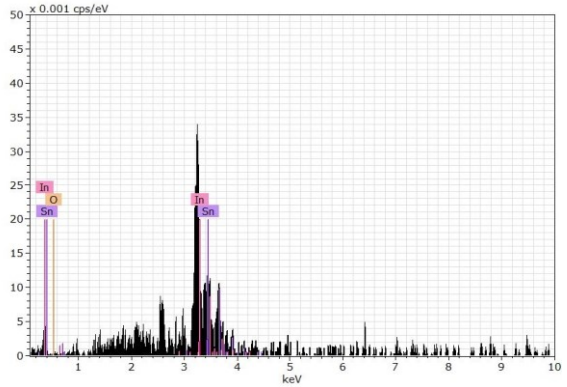

Fig. (3) EDX spectrum of $InSnO_2$ film sample

The optical properties of $InSnO_2$ thin films were examined using UV-visible spectroscopy at room temperature. These measurements are crucial for evaluating the absorption coefficient and estimating the optical energy bandgap. As shown in Fig. (4), the absorption spectrum of the $InSnO_2$ nanostructured film displays an absorption edge in the UV region, and the absorption coefficient (α) was calculated using the following equation [21,22]:

$$\alpha = 2.303 \frac{A}{t} \qquad (2)$$

where A is the absorbance, and t is thin films thickness

For the wavelength range of 300–500 nm, the absorption coefficient (α) is provided in Fig. (5). This coefficient is determined based on the absorbance data. A large and progressive absorption band was seen, which extended from the UV to the visible region. Structural alterations, doping effects, fluctuations in the In/Sn ratio, or changes in carrier concentration and mobility may be the responsible for this behavior, which indicates that the band gap has been reduced and that light absorption has been enhanced. The existence of intermediate energy levels throughout the formation of the film may be another factor that contributes to this tendency.

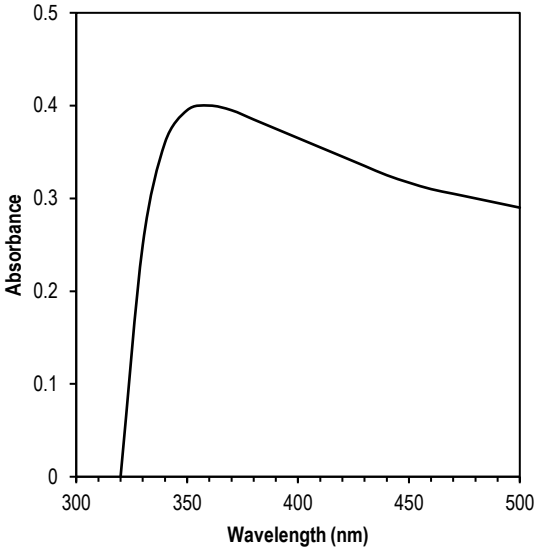

Fig. (4) Absorption spectrum of $InSnO_2$ film sample

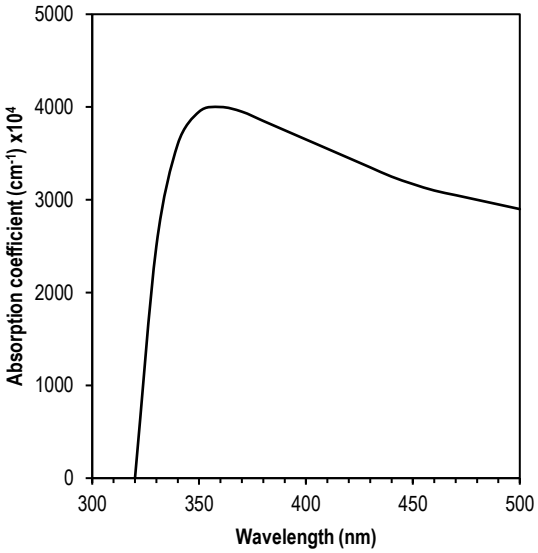

Fig. (5) Absorption coefficient vs. wavelength for $InSnO_2$ nanostructured film sample

Additionally, Tauc's relationship given in Eq. (3) was used in order to determine the magnitude of the optical bandgap. It is seen in Fig. (6) that the combined effect of In_2O_3 and SnO_3 leads to an estimated band gap of about 3.4 eV. The fact that this study demonstrates that the optical properties of $InSnO_2$ films may be altered by altering their composition paves the way for new opportunities in the field of optoelectronic devices, such as TCOs and photodetectors [23].

$$\alpha h\nu = B(h\nu - Eg)^{r} \qquad (3)$$

where hν is the energy of incident photon, B is a constant, E_g is the optical energy gap, and r equals to

 © ALL RIGHTS RESERVED

0.5 for the allowed direct transition, 1.5 for the forbidden direct transition, 2 for the allowed indirect transition, and 2/3 for the forbidden indirect transition

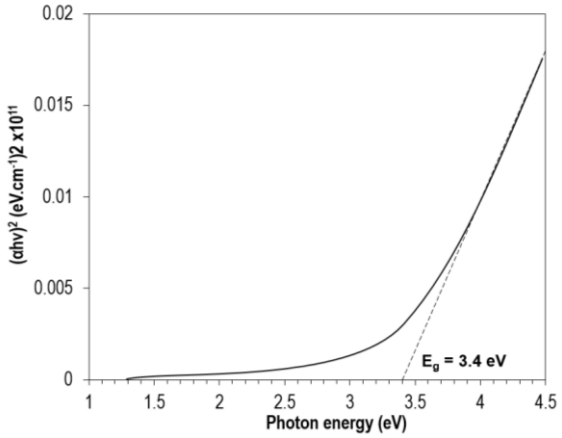

Fig. (6) Plot of $(\alpha h\nu)^2$ vs. (hν) for $InSnO_2$ film sample

The structural properties of $InSnO_2$ in both powder and thin-film forms were examined using X-ray diffraction (XRD) within the 2θ range of 20°-80°, as shown in Fig. (7). The XRD patterns confirmed the polycrystalline nature of both samples, with distinct diffraction peaks corresponding to the (222), (400), (440), and (622) planes, which are consistent with the cubic bixbyite structure of $InSnO_2$. The diffraction peak positions were analyzed using Bragg's equation as [24]:

$$n\lambda = 2d\sin\theta \quad (4)$$

where n is the diffraction order (usually taken as 1), λ is the wavelength of the X-rays, d is the inter-planar spacing, and θ is the diffraction angle

Equation (4) is commonly utilized to determine the lattice parameters and the crystalline structure. This equation describes the rigorous requirements that must be fulfilled for the X-rays, once scattered through the lattice of the crystal, to result in constructive interference. Experimental results establish that the diffraction peaks for the thin film sample deliver significantly higher intensity and resolution. Such notable clarity is specifically evident for the reflection (222) at 30.65°. Such results strongly establish that the sample exhibits higher crystallinity and distinct preferred orientation. It is claimed that the resulting enhanced material properties are due to the interaction between the substrate and the highly regulated deposition process utilized. On the other hand, the powder sample displays peaks that are significantly lower and broader. Such a result indicates a decrease in crystallite size, higher structural disorder, and reduced crystallinity. Such variations are aligned with the relevant synthesis process applied, where thin films are found to contain higher crystallinity due to the deposition and annealing process, in comparison with powder samples that are found to be randomly oriented with higher structural disorder. In aggregate, the XRD analysis confirms that the sample for the thin film exhibits higher crystallinity and preferred orientation of the crystal with respect to the powder sample. This matches with lower full-width at half maximum (FWHM), which translates into larger crystallite size (D), as shown by the Scherrer's equation [25]:

$$D = \frac{0.9\lambda}{\beta\cos\theta} \quad (5)$$

where λ is the wavelength of X-rays (1.5406Å), β is the full-width at half maximum (FWHM) (in radians units), and θ is the diffraction angle (Bragg's angle) of the peak

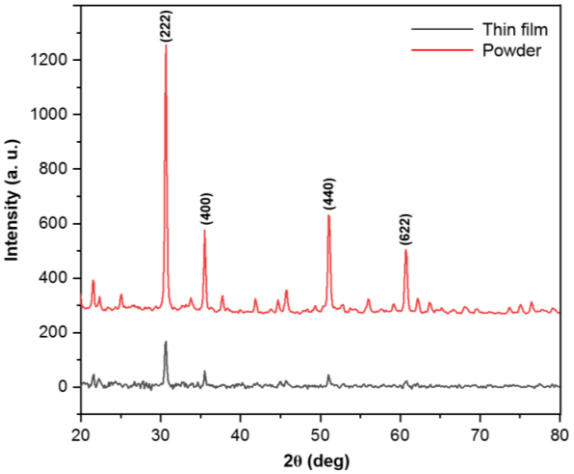

Fig. (7) XRD patterns of $InSnO_2$ powder and thin film prepared by PLD with 200 °C annealing temperature for 60 minutes

Table (1) illustrates the structural parameters of 33nm-thick $InSnO_2$ thin film with average crystallite size of 23.22 nm as calculated by Scherrer's equation.

Table (1) Structural parameters for 33nm-thick $InSnO_2$ nanostructured thin film

(hkl)	Peak Position (2θ)	FWHM (deg)	Crystallite Size D (nm)	Average Crystallite Size (nm)
(222)	30.65	0.3	27.44	23.22
(400)	35.55	0.3	27.79	
(440)	51.05	0.6	14.66	
(622)	60.65	0.4	22.99	

Conversely, the powder form shows broader peaks with lower intensities, which suggest a less ordered structure and smaller crystallite size. The reduced ordering is due to the isotropic and non-oriented nature of powder synthesis methods, which do not have the directed growth of the thin film. These observations suggest that the thin film form of the $InSnO_2$ material is more ordered and crystalline, which would be beneficial for applications in optoelectronic devices, whereas the powder form would be useful in applications where high surface area or catalytic properties are desired.

Atomic force microscopy (AFM) was used in order to evaluate the surface morphology of the $InSnO_2$ thin

 © ALL RIGHTS RESERVED

films. This was done in order to examine the surface architecture, particle distribution, and nanoscale roughness. The 2D AFM image of the $InSnO_2$ thin films on a 3×3 μm^2 region is shown in Fig. (8). A non-uniform topography was seen on the surface, and there were distinct nanoscale granular characteristics.

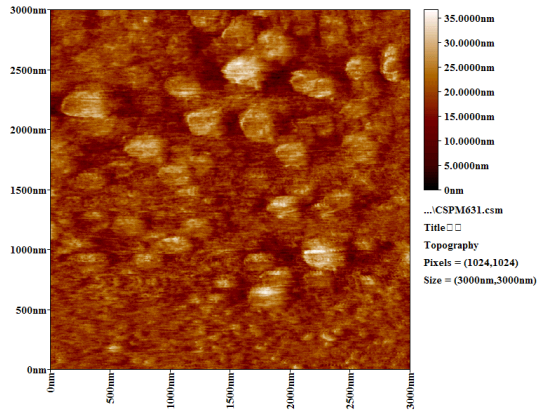

Fig. (8) 2D AFM image of deposited $InSnO_2$ thin film scanned over 3x3 μm^2

Figure (9) depicts the 3D AFM image of the same film. An indication of fast nucleation and localized heating during the deposition process was indicated by the surface morphology, which displayed a granular structure. Applications such as gas sensing, photocatalysis, and optoelectronics may benefit from this granular nanostructure since it has a large surface area, which is favorable. Average particle size, roughness, and root mean square (RMS) values for $InSnO_2$ thin film are shown in table (2).

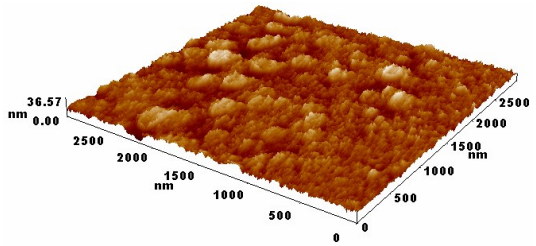

Fig. (9) 3D AFM image of deposited $InSnO_2$ thin films

Table (2) AFM morphology parameters for $InSnO_2$ thin film

Film thickness (nm)	Average particle size(nm)	Roughness Average (nm)	RMS (nm)
33	34.8	3.06	3.99

The surface morphology of the $InSnO_2$ thin film was characterized by SEM at 120,000× magnification. The SEM micrograph in Fig. (10) shows a densely packed granule structure containing virtually spherical nanoparticles with some agglomeration. The particle distribution on the surface appeared to be fairly uniform, indicating a controlled growth process during film deposition.

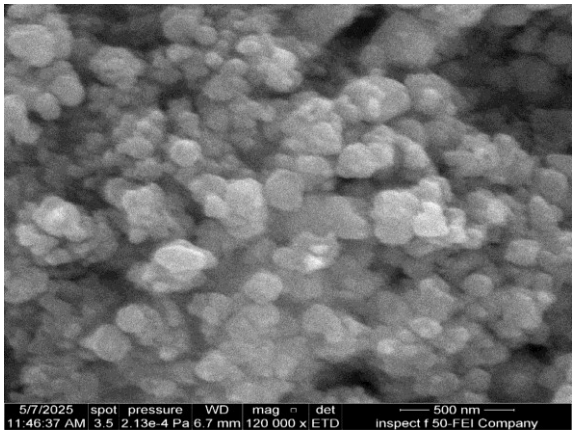

Fig. (10) SEM image of $InSnO_2$ thin film prepared by PLD

The formation of nanocrystalline grains indicates that the PLD method allows the deposition of high-purity, well-adhered thin films with fine structural features. The homogeneity and compactness of the grains will allow for the improvement of the optical and electrical characteristics of the material for device applications such as gas sensors, TCOs, and optoelectronic devices. The indicated homogeneous morphology of the thin film suggests that the PLD was able to provide a continuous and adherent thin film with structural integrity. The nanostructured nature of these films will facilitate the enhancement of the functional properties of the materials with a high surface area and uniform grain boundaries for possible applications in TCOs, devices, or gas sensors due to their uniformity. There were no noticeable surface defects involving cracks or voids, indicating that the quality of the thin-film deposition was successful. These results correspond with previously reported studies of In-based oxide nanostructured films deposited via PLD, which specified that high-purity nanocrystalline films were successfully prepared with the desired surface morphology and a restricted amount of defects [26,27].

The electrical (capacitive-resistive) characteristics of $InSnO_2$ thin film as a humidity sensor device, illustrated in Fig. (1), have been studied.

Figure (11) shows the capacitance (C) of the $InSnO_2$-based humidity sensor examined at three different frequencies (100, 200, and 300 Hz) at room temperature. In the first case, at 100 Hz, the sensor clearly exhibited a linear and consistent increase in capacitance with rising relative humidity (RH%). This suggests that the sensor was highly sensitive, as a strong interaction occurred between the water molecules and the sensor surface. The capacitance is mainly influenced by a mechanism in which the dominant external electric field induces dipole polarization and conformational stress at the interface, particularly at low frequencies. Therefore, at low frequencies (100 Hz), dipolar polarization and

 © ALL RIGHTS RESERVED

interfacial charge accumulation contributed significantly to the sensor response. Moreover, the capacitive reactance (C) plays a crucial role in the behavior of such sensors, especially when varying the frequency. Additionally, the response became significantly steadier and smoother at 200 Hz, with a minor drop in overall sensitivity in comparison to the 100 Hz example, even though linearity was preserved. This was the case despite the fact that the sensor response demonstrated a similar pattern at 200 Hz. The response of the sensor became unstable at 300 Hz, particularly at low humidity levels, when substantial changes in capacitance were detected. This was especially prominent at low humidity levels. There was a modest increasing trend in capacitance at high relative humidity percentages, but the capacitance remained rather steady in the middle of the humidity range. Because of restricted dipole reorientation and decreased water molecule adsorption, the reduction in sensitivity that occurs at high frequencies is caused by a decrease in dielectric relaxation. Previous research has shown that these findings are in agreement with them [28-31].

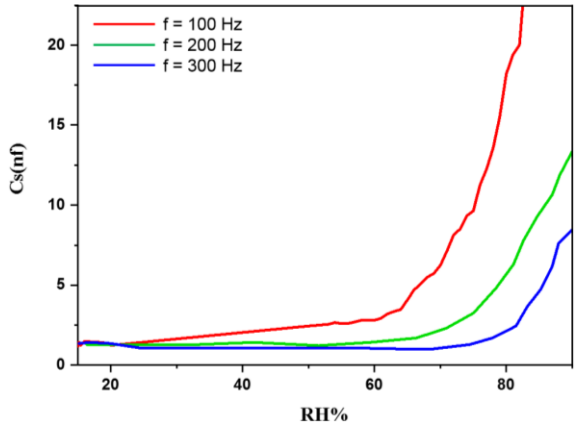

Fig. (11) Capacitance vs. relative humidity for different frequencies

Figure (12) graphs provide an overview of the resistance (R) variation of the $InSnO_2$ sensor material as a function of relative humidity (RH%) at frequencies of 100, 200, and 300 Hz. The optimal trend is characterized by decreasing sensor resistance as RH increases, as seen in all three graphs. The decreasing resistance variation shows the sensor's resistance to the humidity of the material and can be attributed to the adsorption of water on the sensor. With water finding a surface adhesion on the sensor, combined with the enhancement of the protonic conduction in the $InSnO_2$ form, the sensor's overall resistance will be lower at a higher relative humidity.

At a frequency of 100 Hz, resistance showed a fairly steep decrease from 55% to 75% RH, suggesting high sensitivity in this low-frequency regime. The high sensitivity at 100 Hz is likely due to the significant length of time the alternating current is interacting with the adsorbed water molecules, thereby allowing more freedom for charge carrier movement. At 200 Hz, the resistance slope of the curve was slightly less steep, and therefore, the sensitivity moving from 15% to 85% RH will be moderate. Higher frequencies leave less time for polarization and conduction mechanisms to evolve. The slope at 300 Hz is more gradual than at other frequencies and shows evidence of clear signal fluctuations at lower humidity (20-75% RH). This may be caused by a combination of noise sensitivity and diminished dipolar orientation impact related to higher frequencies, which would suggest capacitive effects are increasing and reducing the effective interaction between the sensing material and the humidity-induced charge carriers.

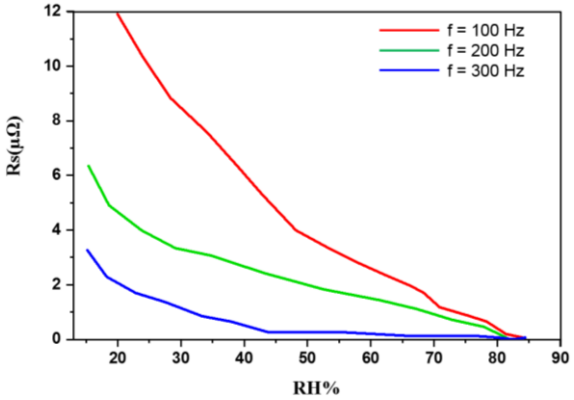

Fig. (13) Resistance vs. relative humidity for different frequencies

4. Conclusions

ITO nanostructured thin films were prepared using the pulsed-laser deposition (PLD) method. The characterization tests verify the crystallinity of the films and the homogeneity of their surfaces. Sensing and electrical properties showed stable response and higher sensitivity at the lower frequencies that confirm that they are reasonable for highly advanced sensing applications.

Acknowledgement

The authors would like to express their sincere thanks to the College of Science, Al-Nahrain University, for providing the academic environment and resources necessary to complete this study.

References

[1] C.G. Granqvist, "Transparent conductors as solar energy materials: A panoramic review", *Sol. Energy Mater.*, 91(17) (2007) 1529-1598.

[2] D.S. Ginley, H. Hosono and D.C. Paine, "Handbook of Transparent Conductors. 2010, Springer Science & Business Media LLC (NY, 2010), p. 548.

[3] E. Fortunato et al., "Transparent Conducting Oxides for Photovoltaics", *MRS Bull.*, 32(3) (2007) 242-247.

 © ALL RIGHTS RESERVED

[4] J. Patel et al., "A Review of Transparent Conducting Films (TCFs): Prospective ITO and AZO Deposition Methods and Applications", *Nanomater.*, 14(24) (2024) 2013.
[5] K.A. Aadim, A.E. Ibrahim and Q.A. Abduljabbar, "Optical and Electrical Properties of $(SnO_2)_X$ (In_2O_3) thin Films Prepared by Pulse Laser Deposition", *Int. J. Phys.*, 5(4) (2017) 116-120.
[6] A. Toikka, M. Ilin and N. Kamanina, "Perspective Coatings Based on Structured Conducting ITO Thin Films for General Optoelectronic Applications", *Coatings*, 14(2) (2024) 178.
[7] V. Rafee et al., "Effect of Sol aging on the structural and optical properties of tin dioxide (SnO_2) nanoparticles and thin films", *Mat. Sci. Eng. B*, 320(10) (2025) 118395.
[8] A.I. Khudiar, M.K. Mohsen and A.M. Oufi, "Laser-induced oxygen vacancies for enhanced gas sensing in zinc oxide thick films", *Radiat. Phys. Chem.*, 238(1) (2026) 113187.
[9] H. Farahani, R. Wagiran and M.N. Hamidon, "Humidity Sensors Principle, Mechanism, and Fabrication Technologies: A Comprehensive Review", *Sensors*, 14(5) (2014) 7881-7939.
[10] Z. Chen and C. Lu, "Humidity Sensors: A Review of Materials and Mechanisms", *Sens. Lett.*, 3(4) (2005) 274-295.
[11] G. Korotcenkov, "Metal oxides for solid-state gas sensors: What determines our choice?", *Mater. Sci. Eng. B*, 139(1) (2007) 1-23.
[12] L. Wang, et al., "Ferroelectric WO_3 Nanoparticles for Acetone Selective Detection", *Chem. Mater.*, 20(15) (2008) 4794-4796.
[13] N. Barsan and U. Weimar, "Conduction Model of Metal Oxide Gas Sensors", *J. Electroceram.*, 7(3) (2001) 143-167.
[14] M. Socol et al., "Pulsed Laser Deposition of Indium Tin Oxide Thin Films on Nanopatterned Glass Substrates", *Coatings*, 9(1) (2019) 19.
[15] M.T. Hussein et al., "Capacitive-resistive measurements of cobalt-phthalocyanine organic humidity sensors", *Phot. Sens.*, 5(3) (2015) 257-262.
[16] M.T. Hussein, F.A. Hasan and E.K. Hassan, "Studying the responsivity and detectivity of GO/PSi/n-Si photo detector via drop casting technique", *J. Opt.*, 53(3) (2024) 2161-2167.
[17] V. Rajendran et al., "Indium tin oxide thin film preparation and property relationship for humidity sensing: A review", *Eng. Rep.*, 6(3) (2024) e12836.
[18] M. Born and E. Wolf, **"Principles of Optics"**, 7th ed., Cambridge University Press (NY, 2020), p. 992.
[19] H.A. Macleod, **"Thin-Film Optical Filters"**, 5th ed., CRC Press (Boca Raton, 2017), p. 696.
[20] F.L. Pedrotti, L.M. Pedrotti and L.S. Pedrotti, **"Introduction to Optics"**, 3rd ed., Cambridge University Press (Cambridge, 2017).
[21] O.S. Heavens, **"The Optical Properties of Thin Solid Films"**, Dover Books on Physics, Dover Publications Inc. (NY, 1992), p. 288.
[22] E. Hecht, **"Optics"**, 5th ed, Pearson (2017) p. 728.
[23] S.M. Sze and K.K. Ng, **"Physics of Semiconductor Devices"**, John Wiley & Sons, Inc. (Hoboken, 2007), p. 763.
[24] B.D. Cullity and S.R. Stock, **"Elements of X-Ray Diffraction"**, 3rd ed., Pearson (NJ, 2001), p. 696.
[25] H.P. Klug and L.E. Alexander, **"X-Ray Diffraction Procedures: For Polycrystalline and Amorphous Materials"**, 2nd ed., Wiley India (NY, 2015), p. 992.
[26] S. Khan et al., "Light trapping by hydrothermally deposited zinc oxide nanostructures with high haze ratio", *Mater. Sci. Semicond. Process.*, 37(9) (2015) 51-56.
[27] T. Ohnishi, H. Koinuma and M. Lippmaa, "Pulsed laser deposition of oxide thin films", *Appl. Surf. Sci.*, 252(7) (2006) 2466-2471.
[28] B. Li et al., "High sensitivity portable capacitive humidity sensor based on In_2O_3 nanocubes-decorated GO nanosheets and its wearable application in respiration detection", *Sens. Actuat. B: Chem.*, 299(11) (2019) 126973.
[29] W. Langgemach, M. Fahland and E. Rädlein, "The influence of sputter-deposited indium tin oxide thin films on the strength of ultra-thin glass", *Open Ceram.*, 21(3) (2025) 100710.
[30] J.R. McGhee et al., "Humidity Sensing Properties of Transparent Sputter-Coated Indium–Tin Oxide and Printed Polymer Structures", *IEEE Sens. J.*, 18(18) (2018) 7358-7364.
[31] J.R. McGhee et al., "Printed, Fully Metal Oxide, Capacitive Humidity Sensors Using Conductive Indium Tin Oxide Inks", *ACS Appl. Electron. Mater.*, 2(11) (2020) 3593-3600.

 © ALL RIGHTS RESERVED